MNRAS **000**, 000–000 (0000) Preprint 19 February 2024 Compiled using MNRAS LATEX style file v3.0

Hot Corona Properties of Swift/BAT detected AGN

Chan Wang, Li-Ming Yu, Wei-Hao Bian*, Bi-Xuan Zhao
School of Physics and Technology, Nanjing Normal University, Nanjing 210046, China

arXiv:1905.08428v1 [astro-ph.HE] 21 May 2019

Accepted XXX. Received YYY; in original form 19 February 2024

ABSTRACT

Using a sample of 208 broad-line active galactic nuclei (AGNs) from Swift/BAT AGN Spectroscopic Survey in ultra-hard X-ray band ($14-195$ keV), the hot corona properties are investigated, i.e. the fraction of gravitational energy dissipated in the hot corona and the hard X-ray photon index. The bolometric luminosity, $L_{\rm Bol}$, is calculated from host-corrected luminosity at 5100 Å. Virial supermassive black hole masses (SMBH, $M_{\rm BH}$) are calculated from the Hβ line width and the corresponding broad line region size-luminosity empirical relation at 5100 Å. We find a strong anti-correlation between the fraction of energy released in corona ($F_{\rm X} \equiv L_{14-195{\rm keV}}/L_{\rm Bol}$) and the Eddington ratio ($\varepsilon \equiv L_{\rm Bol}/L_{\rm Edd}$), $F_{\rm X} \propto \varepsilon^{-0.60\pm0.1}$. It is found that this fraction also has a correlation with the SMBH mass, $F_{\rm X} \propto \varepsilon^{-0.74\pm0.14} M_{\rm BH}^{-0.30\pm0.03}$. Assuming that magnetic buoyancy and feild reconnection lead to the formation of a hot corona, our result favours the shear stress tensor being a proportion of the gas pressure. For our entire sample, it is found that the hard X-ray photon index Γ has a weak but significant correlation with the Eddington ratio, $\Gamma = 2.17 + 0.21 \log \varepsilon$. However, this correlation is not robust because the relation is not statistically significant for its subsample of 32 RM AGNs with relatively reliable $M_{\rm BH}$ or its subsample of 166 AGNs with single-epoch $M_{\rm BH}$. We do not find a statistically significant relation between the photon index and the Eddington ratio taking into account an additional dependence on $F_{\rm X}$.

Key words: accretion, accretion disks - galaxies: active - magnetic fields

1 INTRODUCTION

One of the main purposes of studying active galactic nuclei (AGNs) is to find out how basic features of supermassive black hole (SMBH) accretion is related to the radiation field. A model with a hot corona surrounding a cool accretion disk in AGNs is introduced for the X-ray emission through Compton up-scattering the disc UV photons by the relative electrons in the corona (Liang et al. 1979; Haardt & Maraschi 1991). There are some kinds of the corona geometry, such as the hot planes parallel covering the cold accretion disk (e.g. Haardt & Maraschi 1991; Haardt et al. 1994), a hot sphere around its central SMBH (e.g. Zdziarski et al. 1999), and an inner hot sphere plus an inner warm disk (Kubota & Done 2018). A fraction of total dissipated energy is transferred vertically outside the disk, and released in the hot, magnetically dominated corona (e.g. Haardt & Maraschi 1991; Svensson & Zdziarski 1994). The magnetic field turbulence have been realized in the transportation of angular momentum and formation of the hot corona (e.g. Merloni & Fabian 2002; Wang et al. 2004).The magnetic stress $t_{r\phi}$ is assumed be capable of transporting the angular momentum in the disk. Therefore, the fraction of $F_{\rm X} \equiv L_{\rm X}/L_{\rm Bol}$ ($L_{\rm X}$ and $L_{\rm Bol}$ are the X-ray luminosity and the bolometric luminosity respectively) can be obtained if the magnetic stress and energy transportation are assumed (e.g. Merloni & Fabian 2002). This may give us a possible opportunity to test the working magnetic stress from hard X-ray observations.

The relation between the fraction of energy dissipated in the corona $F_{\rm X}$ and the Eddington ratio ε ($\varepsilon \equiv L_{\rm Bol}/L_{\rm Edd}$, $L_{\rm Edd}$ is the Eddington luminosity) was investigated by some authors (e.g. Merloni & Fabian 2002; Wang et al. 2004; Yang et al. 2006). For a compiled sample of 56 AGNs from *ASCA* observation, Wang et al. (2004) found a relation between $F_{\rm X}$ and ε as $F_{\rm X} \propto \varepsilon^{-0.64\pm0.09}$, where the X-ray luminosity in $2-10$ keV is used. Considering a larger sample of 98 AGNs, Yang et al. (2006) found $F_{\rm X} \propto \varepsilon^{-0.66}$. These results supported the magnetic stress tensor being the form of $t_{r\phi} \propto P_{\rm gas}$, where $P_{\rm gas}$ is the gas pressure. In their compiled sample, they only have nine sources with ultra-hard X-ray observations of INTEGRAL and Swift, and for other sources the luminosity in $2-150$ kev is extrapolated from the 2-10 keV luminosity with a fixed photon index. A sample of more AGNs with direct harder X-ray than 2-10 keV is needed for further investigation, such as Swift/BAT.

Another relation between the X-ray photon index Γ and

* E-mail: whbian@njnu.edu.cn

© 0000 The Authors

the Eddington ratio ε was extensively discussed by using different AGNs samples and by models (e.g. Bian et al. 2003; Wang et al. 2004; Yang et al. 2006; Brightman et al. 2013; Liu et al. 2015; Meyer-Hofmeister et al. 2017; Trakhtenbrot et al. 2017). Trakhtenbrot et al. (2017) recently used a sample of 228 hard X-ray selected low-redshift AGNs drawn from the Swift/BAT AGN Spectroscopic Survey (BASS) to investigate this relation. They found a weak but significant correlation between them, $\Gamma = log(\varepsilon^{0.167})$, and a dependence on the method to derive the SMBH mass. Kubota & Done (2018) presented a truncated-disk model including an outer standard cold disk, an inner warm Comptonising region and a hot corona for the broadband spectral energy distribution (SED) of AGNs (e.g., the soft X-ray excess). They suggested that Γ is also related with $F_{\rm X}$, where increasing of $F_{\rm X}$, the curve of $\Gamma - \varepsilon$ relation is lower.

In this paper, we use a large sample of 208 low-redshift broad-line AGNs with harder X-ray (14 - 195 kev) emission from Swift/BAT to further investigate the corona properties. The sample is based on the Swift BASS catalogue which extents harder X-ray at 14-195 keV. This paper is organized as follows. Section 2 presents our sample. Section 3 is data analysis. Section 4 is our discussion. Section 5 summaries our results. All of the cosmological calculations in this paper assume $\Omega_\Lambda = 0.7$, $\Omega_{\rm M} = 0.3$, and $H_0 = 70$ km s^{-1}Mpc^{-1}.

2 THE SAMPLE

A sample of AGNs used here is selected from Swift BASS drawn from a Swift/BAT 70-month catalogue. The Swift/BAT survey has an all-sky survey in the ultra-hard X-ray band (14-195 kev) which increases the all-sky sensitivity by a factor of 20 compared to previous satellites, such as HEAO 1 (Baumgartner et al. 2013; Koss et al. 2017). Most of the Swift/BAT detected AGNs are nearby ($z < 0.05$), these bright and nearby AGNs offer the best opportunity for studies of corona properties of AGNs with information at ultra-hard X-ray band.

For the Swift BASS, the optical spectroscopic of Swift/BAT sources (642/836) are from dedicated observations and public archival data (Koss et al. 2017). According to Ricci et al. (2017a), compared to the number found at the optical band, the number of broad-line AGNs decreases significantly at the ultra-hard X-ray band. This is due to optical central obscuration for these Swift BASS broad-line AGNs. The X-ray data and the analysis were presented by Ricci et al. (2017b), and we briefly introduce as bellow. For the BASS sample, the analysis by covered the observed-frame energy range of $0.3 - 150$ keV, included all the X-ray data available, including Swift/XRT, XMM-Newton/EPIC, Chandra/ACIS, Suzaku/XIS, or ASCA/GIS/SIS observations. The data were modeled with a set of models that rely on an absorbed power-law X-ray SED with a high-energy cut-off, and a reflection component, as well as additional components accounting for warm absorbers, soft excess, Fe Kα lines, and/or other spectral features. The typical uncertainty on the hard X-ray photon index is less than 0.3 (Ricci et al. 2017b; Trakhtenbrot et al. 2017). There are 227 Swift/BAT detected broad-line AGNs with measured broad Hβ FWHM and the luminosity in 5100 Å. Excluding 19 beamed sources (Koss et al. 2017), our sample is finally composed of 208 Swift/BAT detected broad-line AGNs. For our sample, the mean value of the uncertainty on the hard X-ray photon index ($\Delta\Gamma$) is 0.15 with a standard deviation of 0.02 [1]. There are 193 AGNs with $\Delta\Gamma < 0.4$. Considering the number counts larger than 1000 and $0.01 < z < 0.05$, Trakhtenbrot et al. (2017) presented a sample of 288 AGNs selected from the Swift/BAT to investigate the relation between the hard X-ray photon index and the Eddington ratio. There is a subsample of 126 AGNs with single-epoch spectrum of the Hβ broad line in their sample.

The monochromatic luminosity at 5100 Å in the rest frame, L_{5100}, and the full-width at half-maximum (FWHM) of Hβ, FWHM$_{\rm H\beta}$ are adopted from the Col. (2) and Col. (4) in Table 9 in Koss et al. (2017). We present the properties of our sample of these broad-line AGNs in Table 1. Col. (1) gives the Swift/BAT 70-month hard X-ray survey ID of the object; Col. (2) is the X-ray luminosity (14-195 keV) in units of erg/s. Col. (1)-(2) are adopted from Table 2 in Koss et al. (2017). Col. (6) gives the photon index of the primary X-ray continuum recovered from the entire energy range (0.3-150 keV) and the full multi-component model, which is adopted from Col. 3 in Table 5 in Ricci et al. (2017b).

In the left panel of Fig. 1, we show $L_{14-195{\rm keV}}$ versus z for our sample. The average value of redshift z is 0.061 with the standard deviation of 0.057. The average value of $\log L_{14-195{\rm keV}}$ is 44.02 with the standard deviation of 0.66 in units of erg s^{-1} . In our sample, there are 32 AGNs with the Hβ lag measured by the reverberation mapping (RM) method (Du et al. 2016). It is a special subsample for their reliable SMBH $M_{\rm BH}$ and host-corrected L_{5100}. There are 8 additional AGNs with measured host velocity dispersion σ_* (Koss et al. 2017). There are 13 narrow-line Seyfert 1 galaxies (NLS1s) with FWHM$_{\rm H\beta}$ $<$ 2000 km/s (e.g. Bian et al. 2003). In Fig. 1, blue squares, green triangles, stars denote RM AGNs, NLS1s, AGNs with σ_* values, respectively.

3 ANALYSIS

3.1 The SMBH mass and the Eddington ratio

We use this sample of 208 Swift/BAT detected broad-line AGNs with ultra-hard 14-195 keV to investigate the relation between the hot corona and the cold accretion disk. For the hot corona, we use two parameters, i.e. the fraction of gravitational energy released in the hot corona and the hard X-ray photon index. The SMBH mass and the Eddington ratio are two key parameters for the SMBH accretion process.

The SMBH masses of broad-line AGNs in our sample are estimated as follows: (1) for 32 RM AGNs, their RM SMBH masses are preferentially adopted from Du et al. (2016); (2) for other 8 AGNs with the stellar velocity dispersion (Koss et al. 2017), their SMBH masses are calculated from $M_{\rm BH} - \sigma_*$ relation (Kormendy & Ho 2013; Koss et al. 2017); (3) for the rest of 168 AGNs, we calculate their single-epoch SMBH masses from the empirical $R_{\rm BLR} - L_{5100}$ relation (Kaspi et al. 2000; Bentz et al. 2013). We first remove

[1] Two AGNs, i.e. SWIFT J1119.5+5132 and SWIFT J1313.6+3650A, have no Γ shown in Ricci et al. (2017b) because they were not observed in the 0.3–10 keV range.

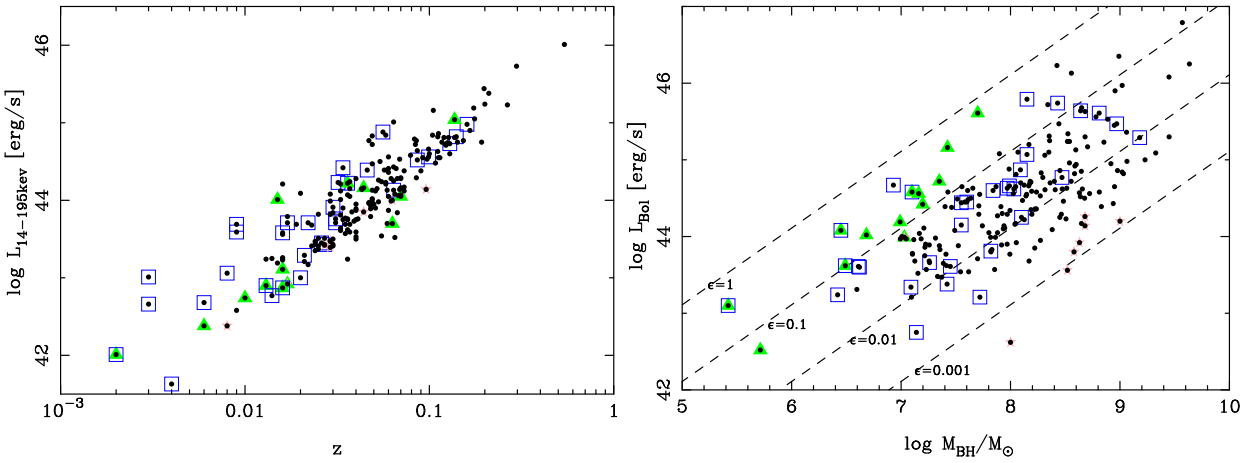


Figure 1. Left: The 14-195 keV X-ray luminosity $L_{14-195\mathrm{keV}}$ vs. redshift z. Right: The bolometric luminosity vs. the SMBH mass. The dash lines show $\varepsilon = L_{\mathrm{Bol}}/L_{\mathrm{Edd}} = 1, 0.1, 0.01, 0.001$, respectively from up to bottom. The black points denote our sample of 208 broad-line Swift/BAT detected AGNs. Green triangles denote 13 NLS1s. Blue squares represent 34 reverberation mapping source in our sample. Stars denote 8 AGNs with stellar velocity dispersion.

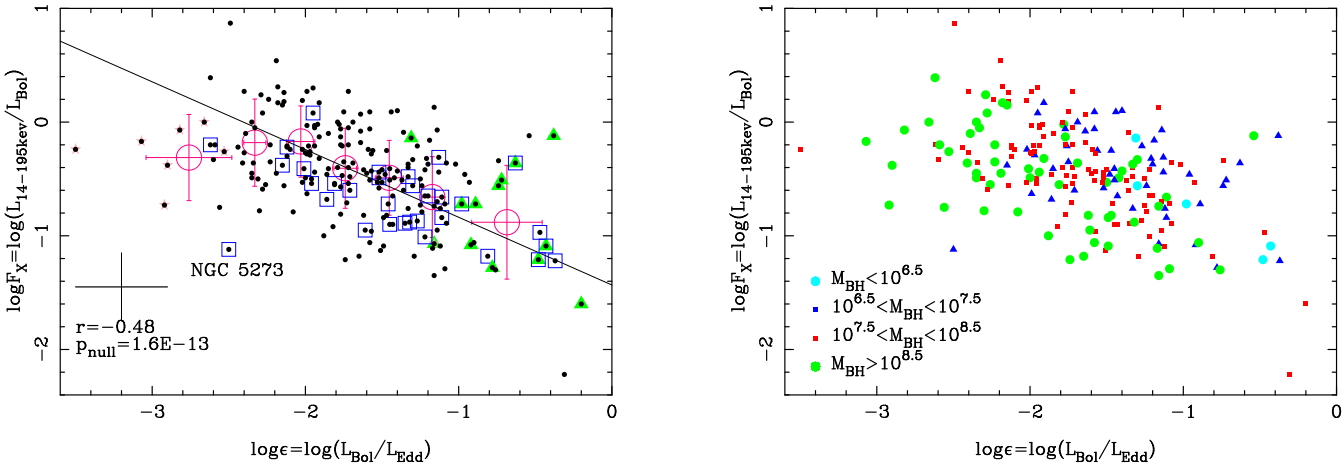


Figure 2. Left: F_{X} vs. ε. The black points denote our sample of 208 broad-line Swift/BAT detected AGNs. The symbols are the same to Figure 1. The open red circles denote 7 binned data. The solid black line is the BCES(Y|X) best-fitting relation. The cross in the lower left corner represents the typical uncertainties of F_{X} and ε. Right: F_{X} and ε relation with different colors denoting different ranges of the SMBH mass.

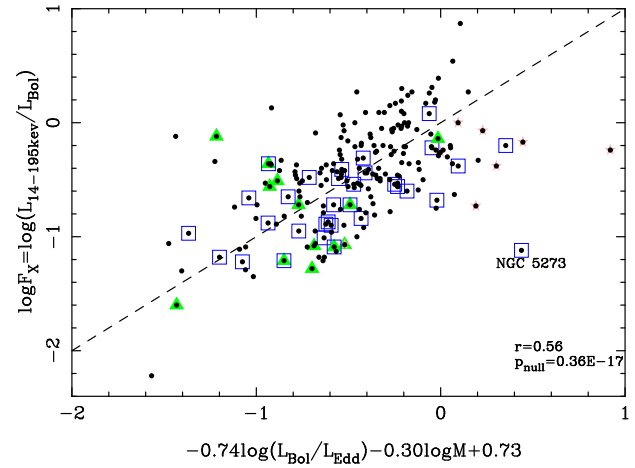


Figure 3. Dependence of F_{X} on the M_{BH} and the ε. The symbols are the same to Figure 1. The dash line is 1:1.

the host contribution in L_{5100} from the empirical formulae by Ge et al. (2016). The host fraction f_{BLR} in the total continuum luminosity at 5100 Å (L_{5100}^{total}) is as follows,

$$f^{\mathrm{host}} = (10.265 \pm 2.92) - (0.225 \pm 0.07) \log L_{5100}^{total} \quad (1)$$

where we do the correction for AGNs with $L_{5100}^{total} \leq 10^{45.6}$erg s^{-1}. The average value of corrected $\log L_{5100}$ is 43.51 with the standard deviation of 0.712. The largest correction of $\log L_{5100}$ is 0.36 dex. For our subsample of 32 RM AGNs, we directly adopt the host-corrected L_{5100} from the image decomposition (Bentz et al. 2013; Du et al. 2016).

Using the Hβ FWHM and the host-corrected L_{5100}, we calculate the single-epoch SMBH mass (Kaspi et al. 2000; Jun et al. 2015; Ge et al. 2016),

$$\begin{aligned} M_{\mathrm{BH}} &= f \times \mathrm{FWHM}_{\mathrm{H}\beta}^2 \times \mathrm{L}_{5100}^{\alpha}/\mathrm{G} \\ &= (8.63 \pm 2.29) \times 10^6 \times L_{5100,44}^{0.533\pm0.034} \mathrm{FWHM}_{\mathrm{H}\beta,3}^2 \ \mathrm{M}_{\odot} \end{aligned} \quad (2)$$

where $\mathrm{FWHM}_{\mathrm{H}\beta,3} = \mathrm{FWHM}_{\mathrm{H}\beta}/10^3\,\mathrm{kms}^{-1}$, $L_{5100,44} =$

$L_{5100}/10^{44}$ erg s^{-1}. In this formulae, the empirical $R_{\rm BLR} - L_{5100}$ relation is adopted from Bentz et al. (2013) where L_{5100} is the host-corrected luminosity at 5100Å, $\alpha = 0.533$, and the factor f is adopted as $f = 1.275$ (Woo et al. 2013). The mean value of $\log(M_{\rm BH}/M_\odot)$ in our sample is 8.00 with the standard deviation of 0.705. For the Swift BASS catalogue, considering the total L_{5100}, the $R_{\rm BLR} - L_{5100}$ relation with $\alpha = 0.65$, $f = 1$, Koss et al. (2017) also calculated the SMBH masses from the single-epoch spectrum for AGNs with broad Hβ lines (Trakhtenbrot et al. 2017). The average value of the mass difference of $\log M_{\rm BH}$ between their calculation and ours is 0.1085 dex. The factor f in our $M_{\rm BH}$ calculation is adopted as $f = 1.275$, the difference of $\log f$ is 0.1055 dex. Therefore, the $M_{\rm BH}$ difference is mainly from different adopted factor f. The difference is smaller than the $M_{\rm BH}$ uncertainty of ~ 0.3 dex.

Using the host-corrected luminosity L_{5100}, we calculate the bolometric luminosity $L_{\rm Bol}$ through the bolometric correction factor at 5100Å (Marconi et al. 2004). Considering AGN SED from IR to X-ray, Marconi et al. (2004) gave a formulae about the bolometric correction factor $f_{\rm bol,b} = L_{\rm Bol}/L_b$ as a function of the bolometric luminosity, where L_b is the luminosity in B band. We use a power-law $f_\nu \propto \nu^{-0.5}$ converting L_b to L_{5100}, and the correction factor formula is,

$$\log(L_{\rm Bol}/L_{5100}) = 0.837 - 0.067\ell + 0.017\ell^2 - 0.0023\ell^3 \quad (3)$$

where $\ell = (\log L_{\rm Bol} - 12)$. Considering the uncertainties of correction factor $\log(L_{\rm Bol}/L_{5100})$ and $\log L_{5100}$ to be 0.1 dex, the uncertainty of $\log L_{\rm Bol}$ is about 0.14 dex (Marconi et al. 2004). For the range of L_{5100} in our sample, $L_{\rm Bol}/L_{5100}$ is $\sim 18.6 - 6.0$ with a larger correction factor for a smaller value of L_{5100}. The Eddington ratio ε are calculated from the $L_{\rm Bol}$ and the SMBH mass, $\varepsilon \equiv L_{\rm Bol}/L_{\rm Edd}$, mainly in the range from -3 to 0 in log ε scale. The uncertainty of log ε is about 0.33 dex. In Fig. 1, we show $L_{\rm Bol}$ versus $M_{\rm BH}$ in the right panel for our sample. The dash lines show $\varepsilon = 1, 0.1, 0.01, 0.001$. We has some AGNs with lower log $\varepsilon < -2.5$ comparing with other samples (Wang et al. 2004; Yang et al. 2006), where most of them have stellar velocity dispersion measurements. For 13 NLS1s, they have large Eddington ratios in our sample (Green triangles in Fig. 1).

3.2 The relation between the fraction of energy released in corona and the SMBH accretion

Using 14-195 keV luminosity by Swift/BAT, we calculate the fraction of energy dissipated in the corona, i.e. $F_{\rm X} \equiv L_{14-195{\rm keV}}/L_{\rm Bol}$. The mean value of log $F_{\rm X}$ is -0.445 with the standard deviation of 0.42. It is slightly larger than the result by Yang et al. (2006), where 10-150 keV luminosity are adopted and which was extrapolated from the 2-10 keV luminosity with a fixed photon index for most of their sources.

The left panel of Fig. 2 shows the $F_{\rm X}$ versus the Eddington ratio. We find that $F_{\rm X}$ has a strong correlation with the Eddington ratio. The Spearman correlation test gives the Spearman correlation coefficient $r = -0.48$ and the probability of the null hypothesis $p_{\rm null} = 1.6 \times 10^{-13}$. We use the bivariate correlated errors and scatter method (BCES; Akritas & Bershady 1996)to perform the linear regression. The BCES(Y|X) best-fitting relation for our total sample is,

$$\log F_X = -(0.60 \pm 0.10)\log\varepsilon - (1.43 \pm 0.17). \quad (4)$$

is plotted as solid line in Figure 2. The uncertainties of log F_X and $\log\varepsilon$ are adopted as 0.3 dex, 0.33 dex, respectively. Since both $F_{\rm X}$ and ε have a relation with L_{5100}, we calculate the correlation coefficient between $F_{\rm X}$ and ε when L_{5100} is kept fixed. The partial Kendall correlation coefficient is -0.27, which indicates that $F_{\rm X}$ and ε are related when excluding the influence of L_{5100}. 32 AGNs with RM SMBH masses are shown as open squares in the left panel of Figure 2. The subsample of these 32 RM AGNs follows this relationship and has a small dispersion compared with the total sample, except NGC 5273, which has lowest values of $L_{14-195{\rm keV}}$ and L_{5100}. For this subsample, there is a better correlation between $F_{\rm X}$ and ε than for the entire sample with $r = 0.53, p_{\rm null} = 1.8 \times 10^{-3}$. 13 NLS1s with large Eddington ratios also follow this correlation for the entire sample. If we exclude these 13 NLS1s from the our sample, we find that $r = -0.46, p_{\rm null} = 2.0 \times 10^{-11}$. Based on ε, we divide the sample into 7 bins with almost the same number in each bin. The open circles in the left panel of Fig. 2 show the mean values of log$F_{\rm X}$ and $\log\varepsilon$ in each bin; the error bars show their standard deviations. The BCES(Y|X) best-fitting relation for binned data is $\log F_{\rm X} = -(0.354 \pm 0.127)\log\varepsilon - (1.04 \pm 0.218)$, and the $F_{\rm X} - \varepsilon$ relation curve becomes flat at low Eddington ratio. It is noticed that the two binned points in the left panel of Fig. 2 are lower than the entire trend. The flat correlation for binned data is possibly due to the effect of the SMBH mass just as shown in the right panel of Fig. 2.

In the right panel of Fig. 2, we plot the $F_{\rm X}$ versus ε but with different colors denoting different ranges of the the SMBH mass. It possibly suggests a selection effect on our sample of Swift/BAT, i.e. higher SMBH mass AGNs can be observed for lower Eddington ratio ε. Excluding AGNs with smaller $\varepsilon < 0.01$, the relation between $F_{\rm X}$ and ε is almost the same with $r = -0.44, p_{\rm null} = 1.5 \times 10^{-8}$. If additionally excluding 13 NLS1s, we find that $r = -0.42, p_{\rm null} = 1.6 \times 10^{-7}$. It implies that the selection effect of lower Eddington ratio is not serious in our analysis. From the right panel of Fig. 2, it is clear that the relation $F_{\rm X}$ and ε is indeed affected by $M_{\rm BH}$. When $M_{\rm BH}$ increases, $F_{\rm X}$ decreases. Therefore, we use the multivariate regression analysis to find the correlation between $F_{\rm X}$, ε and $M_{\rm BH}$ in the form: $\log F_X = a + b_1 \log M_{\rm BH} + b_2 \log\varepsilon$. We use the χ^2 as the estimator to find the best values for these fitting parameters (Merloni et al. 2003; Tremaine et al. 2002),

$$\chi^2 = \Sigma_i \frac{(y_i - a - b_1 x_{1i} + b_2 x_{2i})^2}{\sigma_{y_i}^2 + (b_1\sigma_{x_{1i}})^2 + (b_2\sigma_{x_{2i}})^2} \quad (5)$$

,x_1, x_2, y correspond to $\log M_{\rm BH}$, $\log\varepsilon$, $\log F_{\rm X}$ respectively, σ is the corresponding uncertainties. We find the best fit when χ^2 is the minimum. About the errors of fitting parameters a, b_1, b_2, we make the minimum χ^2/n_{dof} unity and then make χ^2-χ^2_{min}=1, which corresponds to the error of 1 σ. And the fitting result is,

$$\log F_{\rm X} = -(0.74^{+0.14}_{-0.14})\log\varepsilon - (0.30^{+0.03}_{-0.03})\log M_{\rm BH} + 0.73^{+0.24}_{-0.25} \quad (6)$$

(see Fig. 3). The uncertainties of $\log M_{\rm BH}$, $\log\varepsilon$, $\log F_{\rm X}$ are

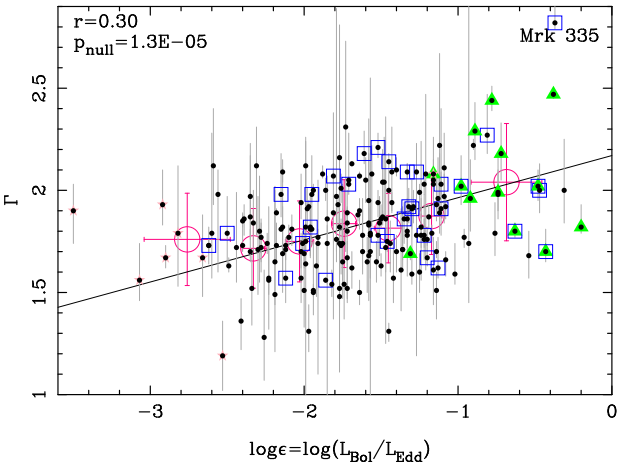


Figure 4. Γ vs. ε. The solid black line is the BCES(Y|X) best-fitting relation. The symbols are the same to Fig. 1.

adopted as 0.3 dex, 0.33 dex, 0.3 dex, respectively. In the multivariate regression, $r = 0.56$, $p_{\rm null} = 3.6 \times 10^{-18}$, which shows that the relationship has been improved after considering the effect of the SMBH mass. For the subsample of 32 RM AGNs, it follows this relationship, except NGC 5273 ($r = 0.53$, $p_{\rm null} = 1.6 \times 10^{-3}$). 13 NLS1s with large Eddington ratios also follow this correlation for the entire sample. This anti-correlation between $F_{\rm X}$ and ε, $M_{\rm BH}$ indicated that the energy released in corona are decreasing with the increasing of the Eddington ratio and the black hole mass, consistent with Fig. 2. Because the Eddington ratio has a dependence on $M_{\rm BH}$, the relation among $F_{\rm X}$, ε and $M_{\rm BH}$ suggests a relation among $F_{\rm X}$, $L_{\rm Bol}$ and $M_{\rm BH}$. Using this χ^2 multivariate regression analysis, we find a relation among $F_{\rm X}$, $L_{\rm Bol}$ and $M_{\rm BH}$,

$$\log F_{\rm X} = -(0.67^{+0.01}_{-0.01}) \log L_{\rm Bol} + (0.57^{+0.04}_{-0.04}) \log M_{\rm BH} + 24.78^{+0.34}_{-0.34} \quad (7)$$

The uncertainties of $\log M_{\rm BH}$, $\log L_{\rm Bol}$, $\log F_{\rm X}$ are adopted as 0.3 dex, 0.14 dex, 0.3 dex, respectively. In this multivariate regression, $r = 0.53$, $p_{\rm null} = 1.1 \times 10^{-16}$.

3.3 The relation between the photon index and the Eddington ratio

Fig. 4 shows the hard X-ray photon index Γ versus the Eddington ratio ε for our Swift/BAT broad-line AGNs. The Spearman correlation coefficient between them is $r = 0.30$ and $p_{\rm null} = 1.3 \times 10^{-5}$. This correlation is statistically significant, albeit weak. The best linear fitting of BCES(Y|X) is,

$$\Gamma = (0.21 \pm 0.05) \log \varepsilon + (2.17 \pm 0.09) \quad (8)$$

The uncertainty of $\log \varepsilon$ is adopted as 0.33 dex. It is consistent with the result by Trakhtenbrot et al. (2017), where the $L_{\rm Bol}$ was estimated from hard X-ray luminosity instead. 13 NLS1s with large Eddington ratios also follow this correlation for the entire sample. If we exclude these 13 NLS1s from our total sample, it makes the parameter range of ε smaller, and we find that the correlation becomes weaker with $r = 0.24, p_{\rm null} = 6.3 \times 10^{-4}$. If excluding AGNs with $\Delta\Gamma > 0.4$ from our total sample, there are 193 AGNs and the correlation becomes slightly stronger with $r = 0.31, p_{\rm null} = 1.2 \times 10^{-5}$. Only for 166 AGNs with single-epoch $M_{\rm BH}$, $r = 0.25, p_{\rm null} = 1.5 \times 10^{-3}$, the correlation is no too significant. Considering the possible effects of spectroscopic aperture (Trakhtenbrot et al. 2017), for our subsample of 80 AGNs at with single-epoch $M_{\rm BH}$ at $0.05 < z < 0.5$, $r = 0.33, p_{\rm null} = 2.7 \times 10^{-3}$. Excluding AGNs with smaller $\varepsilon < 0.01$ from the possible selection effect, this correlation becomes weaker with $r = 0.22, p_{\rm null} = 6.2 \times 10^{-3}$. It is due to smaller parameter range of ε, just like that for NLS1s. Thereofore, for the subsample of AGNs with single-epoch $M_{\rm BH}$, the correlation is not too significant, which is consistent with the result by Trakhtenbrot et al. (2017) (their $p_{\rm null} = 1.1 \times 10^{-3}$). For the subsample of 32 RM AGNs, this correlation is weaker with $r = 0.25, p_{\rm null} = 0.165$. It is consistent with the result by Trakhtenbrot et al. (2017). Mrk 335 is an outline from these 32 RM AGNs, which has a ultra-soft X-ray spectrum (i.e. highest Γ) in our sample.

Based on ε, we also divide the sample into 7 bins with almost the same number in each bin. The open red circles in Fig. 4 show the mean values of Γ and log ε in each bin; the error bars show their standard deviations. It is found that the binned data with the smallest ε seems deviate from this relationship.

For our sample, we also find that Γ has no significant correlation with $L_{\rm Bol}$ ($r = 0.11, p_{\rm null} = 0.11$), or with $M_{\rm BH}$ ($r = -0.11, p_{\rm null} = 0.11$) , which is consistent with the result with Trakhtenbrot et al. (2017).

Considering uncertainties of Γ, ε and $F_{\rm X}$, we also do the χ^2 multivariate regression analysis. However, because of large uncertainties on these parameters, we can not find a suitable multivariate regression with a large $p_{\rm null}$ ($r = 0.07, p_{\rm null} = 0.3$).

4 DISCUSSION

4.1 Energy released in the corona $F_{\rm X}$ and the magnetic stresses tensor

It is assumed that angular momentum transport was carried out by turbulence and that the stress tensor $t_{r\phi}$ was scaled to the disk pressure P, $t_{r\phi} = \alpha P$, α is the viscosity parameter (Shakura & Sunyaev 1973). The viscous stress was suggested to be generally proportional to the magnetic pressure through numerical simulations. It is believed that the strong buoyancy and magnetic field reconnection inevitably lead to the formation of a hot corona (Stella & Rosner 1984). Through magnetic buoyancy, the fraction of gravitational energy dissipated in the hot corona was calculated for different accretion mode (e.g. Merloni & Fabian 2002; Wang et al. 2004; Yang et al. 2006). The relationship between $F_{\rm X}$ and ε can be used to test the working stress of magnetic field turbulence (e.g. Stella & Rosner 1984; Merloni & Fabian 2002; Wang et al. 2004). The fraction of the energy transported by magnetic buoyancy to be $F_{\rm X} = P_{mag} v_p / Q$, where v_p is the transporting velocity, $P_{mag} = B^2/8\pi$ is the magnetic pressure, and the dissipated energy $Q = -(3/2) c_{\rm s} t_{r\phi}$ (Merloni & Fabian 2002). The viscous stress is assumed to scale with magnetic pres-

sure, $t_{r\phi} = -k_0 P_{mag}$, we have

$$F_{\rm X} = \frac{2v_p}{3k_0 c_s} = \frac{2^{\frac{3}{2}} b}{3k_0}\sqrt{\frac{P_{mag}}{P_{tot}}} = \frac{2^{\frac{3}{2}} b}{3k_0^{\frac{3}{2}}}\sqrt{\frac{(-t_{r\phi})}{P_{tot}}} = C\sqrt{\frac{(-t_{r\phi})}{P_{tot}}} \quad (9)$$

where $b = v_p/v_A$, $Alfvén$ velocity $v_A = B/\sqrt{4\pi\rho}$, $P_{tot} = P_{rad} + P_{gas}$, $c_s^2 = P_{tot}/\rho$ and $C = 2^{3/2}b/(3k_0^{3/2}) \sim 1$. Therefore, if the magnetic stress is assumed, we can get the $F_{\rm X}$ at every radius and for different accretion rate. A global value of $< F_{\rm X} >$ can then be obtained by integrating over all the disc area for different magnetic stress tensor (Svensson & Zdziarski 1994; Merloni & Fabian 2002; Wang et al. 2004; Yang et al. 2006). Yang et al. (2006) calculated theoretical light curves for the relation between the factor f and the Eddington ratio for six distinct types of $t_{r\phi}$, which has relations with $P_{gas}, P_{rad}, P_{total}$ (Wang et al. 2004; Yang et al. 2006). The stress tensors of $t_{r\phi}$ are $-\alpha P_{total}$, $-\alpha P_{gas}$, $-\alpha P_{rad}$, $-\alpha\sqrt{P_{rad}P_{total}}$, $-\alpha\sqrt{P_{gas}P_{total}}$, $-\alpha\sqrt{P_{gas}P_{rad}}$ for the models from 1 to 6, respectively. α is the viscosity. Wang et al. (2004) adopted $\alpha = 0.05, 0.1, 0.4$ for $M_{\rm BH} = 10^8 M_\odot$, and $\alpha = 0.05$ but for $M_{\rm BH} = 10^6 M_\odot$. Yang et al. (2006) adopted $\alpha = 0.1, 0.8$ for $M_{\rm BH} = 10^8, 10^6 M_\odot$. Comparing with the calculation by Wang et al. (2004), Yang et al. (2006) considered advection cooling and thermal instability in their calculation. The advection cooling has an effect on $F_{\rm X}$ at dimensionless accretion rate $\dot{m} > 1$ (see right panel in Fig. 5 in Yang et al. 2006). Their results are consistent with each other. Different models have different slope of the $F_{\rm X} - \varepsilon$ relation. This relation is moved along the y-axis of $F_{\rm X}$ for different $M_{\rm BH}$ and α. However, the slope of this relation is not sensitive to them. For model 1, the slope is zero. For model 3 or 4, the slope is positive. For model 2 or 5 the slope is negative. For model 6, the slope changes from a positive value to a negative value (see Fig. 5 in Yang et al. 2006). For all the models, $F_{\rm X}$ is proportional to $\alpha^{0.5}$. Considering our large value of $F_{\rm X}$, large α is needed ($\alpha = 0.8$). We use the slope of the relation between $F_{\rm X}$ and ε to distinguish different models. For their model 2, i.e. magnetic stress tensor $t_{r\phi} \propto P_{gas}$, $F_{\rm X} \propto \varepsilon^{-0.77}$. For their model 5, i.e. magnetic stress tensor $t_{r\phi} \propto \sqrt{P_{gas}P_{total}}$, $F_{\rm X} \propto \varepsilon^{-0.44}$ (see also Wang et al. 2004). For our sample, $F_{\rm X} \propto \varepsilon^{-0.60\pm0.1}$. It is slightly flatter than $-0.64, -0.66$ by Wang et al. (2004); Yang et al. (2006), respectively for AGNs samples with only 2-10 keV data. However, considering the effect of $M_{\rm BH}$, $F_{\rm X} \propto \varepsilon^{-0.74\pm0.14}$. The steeper index of -0.72 favours model 2 in Yang et al. (2006), where the magnetic stress tensor is $t_{r\phi} \propto P_{gas}$.

Comparing with result by Wang et al. (2004), as shown in Fig. 2, we find that the $F_{\rm X} - \varepsilon$ relation depends on the SMBH masses, $F_{\rm X} \propto M_{\rm BH}^{-0.30\pm0.03}$. Differences in $M_{\rm BH}$ may flatten the slope as shown as the binned data in the left panel of Fig. 2. The trend of $M_{\rm BH}$ dependence on the $F_{\rm X} - \varepsilon$ relation is also consistent with the theoretical curves calculated assuming the same viscosity of $\alpha = 0.1$ by Yang et al. (2006) (see their Fig. 5). For AGNs with small SMBH masses, it is expected that $F_{\rm X}$ should be large for these AGNs with the small Eddington ratio $L_{\rm Bol}$ /$L_{\rm Edd}$.

4.2 Hard X-ray Photon index Γ

We present the relation between the hard X-ray photon index Γ and the Eddington ratio ε for our sample of 208 low-reshift broad-line AGNs from Swift BASS catalogue. We find a correlation between Γ and ε: $\Gamma = (2.17 \pm 0.09) + (0.21 \pm 0.05)\log\varepsilon$. The relation index of 0.21 ± 0.05 is consistent with 0.26 ± 0.05, 0.26 ± 0.05, 0.17 ± 0.04 by Bian et al. (2003); Wang et al. (2004); Trakhtenbrot et al. (2017), respectively. Although we find this correlation is significant for our entire sample, the correlation for a subsample of 166 AGNs with sing-epoch $M_{\rm BH}$ or a subsample of 32 RM AGNs with relatively reliable $M_{\rm BH}$ is not significant. Therefore, this relation between Γ and ε is statistically significant but not robust, which depends on the $M_{\rm BH}$ determination method, and more reliable $M_{\rm BH}$ is needed in the future for this correlation analysis. Yang et al. (2015) found a V-type relation between Γ and ε, and the turning point is at $\log\varepsilon \simeq -3$, which is due to the change of the accretion mode. In Fig. 4 we find a possible turning point at $\log\varepsilon \simeq -3$ for our binned data.

According to the study of Kubota & Done (2018), they develop a truncated-disk model for the broad-band SED of AGNs which includes an outer standard disc, an inner warm Comptonising region and a hot corona. The inner warm Comptonising region has different parameters from the corona, in electron temperature ($kT_e \sim 0.1 - 1$ keV vs. $40 - 100$ keV) and the optical depth ($\tau \sim 10 - 25$ vs. $1 - 2$) (Kubota & Done 2018). In their theoretical calculation for this truncated-disk geometry, they found that Γ - $\dot{m}$ relation is affected by $F_{\rm X}$, with the increasing of $F_{\rm X}$, the relation curve of $\Gamma - \dot{m}$ relation is lower (see their Fig. 5), where $\dot{m}$ is the dimensionless accretion rate (i.e. $L_{\rm Bol}$ /$L_{\rm Edd}$ assuming a constant efficient). By employing a multivariate χ^2 regression technique, taking uncertainties into account, we investigate the possible presence of a relation amongst ε, $F_{\rm X}$ and Γ as predicted by the model of a warm Comptonising corona proposed by Kubota & Done (2018). We do not find a statistically significant relation amongst these parameters, which is, at face value, in contradiction with the prediction by Kubota & Done (2018). Yet, we caution that the absence for such a relation in our dataset can be partly due to the large uncertainties on these parameters.

5 CONCLUSIONS

Using a compiled sample of 208 broad-line AGNs from Swift/BAT Spectroscopic Survey with ultra-hard X-ray band (14-195kev) observations, the properties of hot corona are investigated. The main conclusions can be summarized as follows:

- For our sample of low-redshift broad-line AGNs, host-corrected L_{5100} is used to estimate $L_{\rm Bol}$, and empirical $R_{\rm BLR} - L_{5100}$ relation by Bentz et al. (2013) is used to calculate the single-epoch SMBH $M_{\rm BH}$, except for AGNs with measured RM $M_{\rm BH}$ and host stellar velocity dispersion. There is a subsample of 32 RM AGNs with reliable $M_{\rm BH}$ and host-corrected L_{5100}, and a subsample of 13 NLS1s. The fraction of gravitational energy dissipated in the hot corona is estimated from 14-195 keV by Swift,

$F_{\rm X} \equiv L_{14-195{\rm keV}}/L_{\rm Bol}$. For our sample , the mean value of log $F_{\rm X}$ is -0.445 with the standard deviation of 0.42.

• It is found that $F_{\rm X}$ is both correlated with the Eddington ratio and the black hole mass, $F_{\rm X} \propto \varepsilon^{-0.74\pm0.14} M_{\rm BH}^{-0.30\pm0.03}$, which indicates that the energy released in corona are decreasing with the increasing of the Eddington ratio and the black hole mass. The subsample of 32 RM AGNs also follows this correlation, as well as for 13 NLS1s. Considering magnetic buoyancy and magnetic field reconnection leading to the formation of a hot corona, our result favors the magnetic stress tensor being a proportion of the gas pressure, $t_{r\phi} \propto P_{gas}$, which is consistent with the result by Wang et al. (2004).

• For our total sample, the hard X-ray photon index has a correlation with the Eddington ratio ε, $\Gamma = (2.17\pm0.09) + (0.21\pm0.05)\log\varepsilon$. This correlation is statistically significant, albeit weak. However, this correlation is not robust because the relation for its subsample of 32 RM AGNs with relatively reliable $M_{\rm BH}$ or its subsample of 166 AGNs with single-epoch $M_{\rm BH}$ is not significant. Therefore, the significant of this relation between Γ and ε depends on the $M_{\rm BH}$ determination method and more reliable $M_{\rm BH}$ is needed in the future for this correlation analysis. Considering large uncertainties of ε, $F_{\rm X}$ and Γ, from the χ^2 multivariate regression analysis, we do not find a statistically significant relation between the photon index and the Eddington ratio taking into account an additional dependence on $F_{\rm X}$.

ACKNOWLEDGEMENTS

We are very grateful to Wang Jian-Min for the instructive comments. We are also very grateful to the anonymous referee for her/his instructive comments which significantly improved the content of the paper. This work is supported by the National Key Research and Development Program of China (No. 2017YFA0402703). This work has been supported by the National Science Foundations of China (Nos. 11373024, 11233003, and 11873032).

REFERENCES

Akritas M. G., Bershady M. A., 1996, ApJ, 470, 706
Baumgartner W. H., Tueller J., Markwardt C. B., Skinner G., Barthelmy S., Mushotzky R. F., Evans P. A., Gehrels N., 2013, ApJS, 207, 19
Bentz M. et al., 2013, ApJ, 767, 149
Bentz M., Horenstein D., Bazhaw C. et al., 2014, ApJ, 796, 8
Bian W., Zhao Y., 2003, MNRAS, 343, 164
Brightman M. et al., 2013, MNRAS, 433, 2485
Pu Du., Wang J. -M., Hu C. et al., 2016, ApJL, 818, L14
Ge X., Bian W. H., Jiang X. L. et al., 2016, MNRAS, 462, 966
Haardt F., Maraschi L., 1991, ApJ, 380, L51
Haardt F., Maraschi L., Ghisellini G., 1994, ApJL, 432, L95
Kaspi S., Smith P. S., Netzer H., et al., 2000, ApJ, 533, 631
Jun H. D. et al., 2015, ApJ, 806, 109
Kormendy J., Ho L. C., 2013, ARA&A, 51, 511
Koss M., Trakhtenbrot B., Ricci C. et al., 2017, ApJ, 850, 74
Kubota A., Done C., 2018, MNRAS, 480, 1247, arxiv:1804.00171
LaValley M. P., Isobe T., Feigelson E. D., 1992, BAAS, 24, 839
Liang E. et al., 1979, ApJL, 231, L111
Liu B.-F., et al., 2015, ApJ, 806, 223
Marconi A., Risaliti G., Gilli R. et al., 2004, MNRAS, 351, 169
Merloni A., Fabian A. C., 2002, MNRAS, 332, 165 (MF02)
Merloni A., Heinz S., Di Matteo T., 2003, MNRAS, 345, 1057
Meyer-Hofmeister E. et al., 2017, A&A, 607, 94
Ricci C., Trakhtenbrot B., Koss M. et al., 2017a, Nature 549, 488
Ricci C., Trakhtenbrot B., Koss M. et al., 2017b, ApJs, 233, 17
Shakura N. I., Sunyaev R. A., 1973, A&A, 24, 337
Stella L., Rosner R., 1984, ApJ, 277, 312
Svensson R., Zdziarski A. A., 1994, ApJ, 436, 599
Trakhtenbrot B., Ricci C., Koss M. J. et al., 2017, MNRAS, 470, 800, arxiv:1705.01550
Tremaine S. et al., 2002, ApJ, 574, 740
Wang J. -M., Watarai K. -Y., Mineshige S., 2004, ApJ, 607, L107
Woo J.-H., Schulze, A., Park, D. et al., 2013, ApJ, 772, 49
Yang F., Hu C., Chen Y. et al., 2006, ChJAA, 7, 353
Yang Q. et al., 2015, MNRAS, 447, 1692
Zdziarski A. A., Lubinski P., and Smith D. A., 1999, MNRAS, 303, L11

Table 1. A sample of 208 broad-line AGNs detected by Swift BAT.
Col.(1): Swift/BAT 70-month hard X-ray survey ID; Col.(2-3): The luminosity of hard X-ray in 14-195 keV and host-corrected 5100 Å in units of erg/s; Col.(4): The bolometric luminosity $L_{\rm Bol}$ in units of erg/s; Col.(5): Black hole mass; Col.(6): The photon index adopted from (Ricci et al. 2017b); Col.(7): Notes, D: L_{5100} from Du et al. (2016); K: L_{5100} from Koss et al. (2017); 1: $M_{\rm BH}$ from Du et al. (2016); 2: $M_{\rm BH}$ from the $M_{\rm BH}-\sigma_*$ relation with measured σ_* (Kormendy & Ho 2013; Koss et al. 2017); 0: $M_{\rm BH}$ from the single-epoch spectrum in this work.

ID	$\log L_{\rm x(14-195kev)}$ erg s^{-1}	$\log L_{5100}$ erg s^{-1}	$\log L_{\rm Bol}$ erg s^{-1}	$\log M_{\rm BH}$ M$_\odot$	Γ	Notes
(1)	(2)	(3)	(4)	(5)	(6)	(7)
6	43.45	43.76	44.67	6.93	$2.82^{+0.08}_{-0.03}$	D 1
16	44.82	44.97	45.79	8.15	$2.00^{+0.13}_{-0.11}$	D 1
36	44.41	43.13	44.11	7.95	$1.81^{+0.36}_{-0.08}$	K 0
39	44.98	44.81	45.64	8.64	$2.03^{+0.37}_{-0.06}$	D 1
43	43.19	42.40	43.48	7.33	$1.92^{+0.03}_{-0.02}$	K 0
60	43.97	42.87	43.88	7.35	$1.68^{+0.50}_{-0.22}$	K 0
61	44.26	42.99	43.99	7.86	$1.82^{+0.28}_{-0.06}$	K 0
73	44.39	43.98	44.87	8.09	$2.09^{+0.04}_{-0.03}$	D 1
77	42.92	42.99	43.99	7.03	$2.08^{+0.18}_{-0.08}$	K 2
94	43.41	42.74	43.77	7.99	$1.52^{+0.16}_{-0.18}$	K 0
99	43.93	43.71	44.63	7.65	$1.93^{+0.13}_{-0.08}$	K 0
106	44.15	43.62	44.55	8.15	$1.84^{+0.08}_{-0.06}$	K 0
111	44.60	44.21	45.09	9.33	$1.97^{+0.26}_{-0.21}$	K 0
113	44.47	43.80	44.71	8.19	$1.65^{+0.12}_{-0.15}$	K 0
116	43.43	43.50	44.44	7.55	$1.78^{+0.08}_{-0.06}$	D 1
127	44.05	43.63	44.56	8.03	$1.83^{+0.26}_{-0.14}$	K 0
129	43.56	42.74	43.77	7.41	$2.01^{+0.07}_{-0.07}$	K 0
130	42.87	43.10	44.08	6.45	$2.02^{+0.08}_{-0.07}$	D 1
134	44.14	43.19	44.17	8.05	$2.12^{+0.14}_{-0.23}$	K 0
147	44.72	42.83	43.85	8.22	$1.63^{+0.04}_{-0.03}$	K 0
162	43.64	43.44	44.39	8.83	$1.98^{+0.12}_{-0.38}$	K 0
167	44.41	43.25	44.22	8.13	$1.94^{+0.14}_{-0.08}$	K 0
169	43.99	43.61	44.53	8.14	$1.80^{+0.20}_{-0.16}$	K 0
183	44.24	43.75	44.66	8.17	$1.70^{+0.26}_{-0.11}$	K 0
190	43.59	43.35	44.30	7.92	$2.31^{+0.42}_{-0.61}$	K 0
197	43.57	42.98	43.98	7.31	$1.31^{+0.04}_{-0.05}$	K 0
213	43.89	43.34	44.29	7.97	$1.97^{+0.92}_{-0.27}$	K 0
214	44.83	44.38	45.25	8.36	$1.76^{+0.22}_{-0.10}$	K 0
220	44.84	44.34	45.20	8.17	$1.92^{+0.05}_{-0.06}$	K 0
223	43.52	43.73	44.65	8.05	$1.84^{+0.13}_{-0.16}$	K 0
224	44.16	44.07	44.95	8.92	$1.81^{+0.07}_{-0.08}$	K 0
228	43.69	43.55	44.48	7.61	$1.78^{+0.46}_{-0.22}$	K 0
230	43.75	43.29	44.25	8.45	$2.12^{+0.19}_{-0.34}$	K 0
232	43.85	43.40	44.35	8.19	$1.81^{+0.17}_{-0.13}$	K 0
242	43.23	42.39	43.47	7.37	$1.70^{+0.09}_{-0.08}$	K 0
244	44.08	43.41	44.36	8.24	$1.75^{+0.09}_{-0.07}$	K 0
254	44.21	44.23	45.10	8.07	$1.66^{+0.04}_{-0.08}$	K 0
261	43.79	42.56	43.62	7.42	$1.77^{+0.04}_{-0.02}$	K 0
266	44.23	43.87	44.77	8.47	$2.07^{+0.04}_{-0.04}$	D 1
269	43.24	42.48	43.54	7.54	$1.73^{+0.02}_{-0.01}$	K 0
274	44.02	44.36	45.23	8.85	$1.54^{+0.08}_{-0.17}$	K 0
285	43.35	42.64	43.68	8.17	$1.79^{+0.49}_{-0.22}$	K 0
291	43.21	42.97	43.97	7.18	$1.80^{+0.16}_{-0.08}$	K 0
301	42.58	42.09	43.21	7.09	$1.64^{+0.60}_{-0.65}$	K 0
310	44.09	43.16	44.14	7.74	$1.89^{+0.02}_{-0.02}$	K 0
313	43.90	42.97	43.97	6.99	$1.70^{+0.05}_{-0.03}$	K 0
314	45.04	44.29	45.16	7.42	$2.47^{+0.02}_{-0.02}$	K 0
316	44.21	43.44	44.39	7.91	$1.50^{+0.06}_{-0.06}$	K 0
318	44.38	43.65	44.58	8.24	$1.82^{+0.73}_{-0.36}$	K 0
338	44.55	44.18	45.06	8.31	$1.61^{+0.30}_{-0.20}$	K 0
347	43.69	43.69	44.61	8.32	$1.54^{+0.07}_{-0.06}$	K 0
363	43.87	43.93	44.83	8.28	$1.70^{+0.85}_{-1.02}$	K 0
376	44.75	44.62	45.47	8.44	$1.97^{+0.11}_{-0.13}$	K 0
378	43.50	43.45	44.40	7.71	$2.09^{+0.22}_{-0.19}$	K 0
382	43.71	43.68	44.60	7.84	$1.86^{+0.08}_{-0.12}$	D 1
384	43.43	42.64	43.68	7.12	$2.08^{+0.14}_{-0.26}$	K 0
389	43.47	43.23	44.20	9.00	$1.93^{+0.17}_{-0.10}$	K 2

Table 1. –continu

ID	$\log L_{\rm x(14-195kev)}$ erg s^{-1}	$\log L_{5100}$ erg s^{-1}	$\log L_{\rm Bol}$ erg s^{-1}	$\log M_{\rm BH}$ M$_\odot$	Γ	Notes
(1)	(2)	(3)	(4)	(5)	(6)	(7)
394	44.75	44.44	45.30	9.45	$1.28^{+0.33}_{-0.21}$	K 0
398	44.28	43.81	44.72	8.55	$1.51^{+0.03}_{-0.03}$	K 0
403	43.96	42.99	43.99	7.82	$1.50^{+0.25}_{-0.11}$	K 0
409	44.56	44.91	45.74	8.43	$2.27^{+0.20}_{-0.09}$	D 1
411	43.75	42.95	43.96	7.12	$1.78^{+0.23}_{-0.59}$	K 0
418	44.74	43.57	44.50	8.68	$1.80^{+0.27}_{-0.25}$	K 0
420	44.55	44.11	45.00	9.23	$1.87^{+0.30}_{-0.10}$	K 0
425	45.44	44.45	45.31	8.35	$2.03^{+0.08}_{-0.10}$	K 0
431	44.81	44.51	45.36	9.06	$1.89^{+0.49}_{-0.52}$	K 0
443	43.69	42.72	43.75	7.22	$1.84^{+0.07}_{-0.07}$	K 0
447	44.39	44.85	45.68	8.65	$2.11^{+0.17}_{-0.20}$	K 0
449	43.82	43.92	44.82	8.59	$2.08^{+0.04}_{-0.02}$	K 0
455	44.01	43.43	44.38	7.46	$1.76^{+0.06}_{-0.03}$	K 0
458	44.22	43.66	44.58	7.10	$1.80^{+0.04}_{-0.03}$	D 1
459	43.53	43.38	44.34	7.99	$2.16^{+0.65}_{-1.05}$	K 0
460	43.48	43.05	44.04	7.17	$1.82^{+0.14}_{-0.10}$	K 0
461	43.42	42.77	43.80	8.58	$1.67^{+0.06}_{-0.05}$	K 2
466	44.72	43.91	44.81	8.05	$1.71^{+0.21}_{-0.09}$	K 0
470	43.17	42.45	43.52	7.15	$1.65^{+0.38}_{-0.18}$	K 0
473	44.64	43.63	44.56	8.72	$1.77^{+0.09}_{-0.12}$	K 0
481	43.24	43.00	44.00	7.01	$1.89^{+0.29}_{-0.10}$	K 0
495	43.70	43.34	44.29	8.46	$1.72^{+0.12}_{-0.12}$	K 0
497	42.66	42.24	43.34	7.09	$1.56^{+0.01}_{-0.01}$	D 1
501	44.77	44.44	45.30	8.68	$1.86^{+0.07}_{-0.04}$	K 0
507	44.36	43.70	44.62	8.47	$1.31^{+0.13}_{-0.10}$	K 0
512	43.89	43.18	44.16	8.04	$1.69^{+0.08}_{-0.07}$	K 0
524	43.62	42.81	43.83	7.83	$1.71^{+0.06}_{-0.05}$	K 0
529	44.75	44.37	45.24	8.54	$1.57^{+0.19}_{-0.12}$	K 0
530	43.59	42.79	43.81	7.82	$1.57^{+0.13}_{-0.12}$	D 1
532	43.39	42.50	43.56	8.52	$1.56^{+0.18}_{-0.10}$	K 2
537	44.48	43.69	44.61	8.41	...	K 0
542	43.29	42.55	43.60	6.62	$1.62^{+0.15}_{-0.05}$	D 1
549	43.85	42.92	43.92	8.63	$1.79^{+0.33}_{-0.26}$	K 2
550	46.01	45.32	46.13	8.56	$1.68^{+0.12}_{-0.11}$	K 0
552	43.43	42.88	43.89	7.26	$2.04^{+0.22}_{-0.17}$	K 0
556	44.28	43.79	44.70	8.09	$1.63^{+0.06}_{-0.05}$	K 0
558	43.69	42.56	43.61	7.45	$1.98^{+0.04}_{-0.04}$	D 1
561	44.25	43.73	44.65	7.87	$1.86^{+0.04}_{-0.08}$	K 0
565	43.73	42.94	43.95	8.27	$1.72^{+0.27}_{-0.17}$	K 0
566	42.38	41.25	42.52	5.71	$1.69^{+0.03}_{-0.03}$	K 0
567	44.12	43.65	44.58	7.43	$1.77^{+0.04}_{-0.05}$	K 0
572	44.14	43.71	44.63	8.51	$1.51^{+0.31}_{-0.18}$	K 0
575	44.14	43.16	44.14	8.68	$1.67^{+0.21}_{-0.19}$	K 2
576	43.95	43.51	44.45	7.58	$1.99^{+0.04}_{-0.11}$	K 0
583	43.00	42.29	43.38	7.42	$1.98^{+0.20}_{-0.11}$	D 1
585	42.01	41.96	43.10	5.42	$1.70^{+0.11}_{-0.05}$	D 1
587	44.90	44.03	44.92	8.59	$1.93^{+0.05}_{-0.10}$	K 0
589	44.00	43.30	44.26	8.68	$1.19^{+0.17}_{-0.17}$	K 2
595	43.01	42.09	43.21	7.72	$1.73^{+0.03}_{-0.03}$	D 1
596	43.41	42.87	43.88	7.52	$1.73^{+0.13}_{-0.14}$	K 0
607	42.38	41.37	42.62	8.00	$1.90^{+0.13}_{-0.16}$	K 2
608	42.90	42.57	43.62	6.49	$2.02^{+0.15}_{-0.09}$	D 1
611	44.28	44.80	45.63	8.68	$2.05^{+0.10}_{-0.09}$	K 0
613	43.47	42.67	43.71	7.70	$1.77^{+0.06}_{-0.04}$	K 0
623	44.13	43.70	44.62	8.03	$2.21^{+0.07}_{-0.05}$	D 1
624	44.60	44.08	44.96	8.54	$1.62^{+0.08}_{-0.10}$	K 0
631	43.06	42.62	43.66	7.26	$2.03^{+0.01}_{-0.01}$	D 1
636	43.82	43.11	44.09	8.38	$1.73^{+0.16}_{-0.03}$	K 0
641	42.77	42.56	43.61	6.61	$1.91^{+0.18}_{-0.13}$	D 1
644	44.13	43.79	44.70	8.36	$1.48^{+0.06}_{-0.07}$	K 0
651	44.28	43.73	44.65	7.56	$1.59^{+0.15}_{-0.05}$	K 0
652	43.84	42.51	43.57	7.86	$1.85^{+0.03}_{-0.03}$	K 0
657	43.26	42.74	43.77	7.10	$2.00^{+0.10}_{-0.12}$	K 0

Table 1. –continu

ID	$\log L_{\rm x(14-195kev)}$ erg s^{-1}	$\log L_{5100}$ erg s^{-1}	$\log L_{\rm Bol}$ erg s^{-1}	$\log M_{\rm BH}$ M$_\odot$	Γ	Notes
(1)	(2)	(3)	(4)	(5)	(6)	(7)
663	43.50	43.10	44.08	7.49	$1.94^{+0.06}_{-0.07}$	K 0
664	43.84	43.06	44.05	7.88	...	K 0
667	44.29	43.73	44.65	8.95	$1.36^{+0.11}_{-0.14}$	K 0
683	43.95	43.44	44.39	7.40	$1.96^{+0.20}_{-0.07}$	K 0
686	41.63	41.54	42.75	7.14	$1.79^{+0.18}_{-0.16}$	D 1
689	44.29	43.81	44.72	8.18	$1.78^{+0.18}_{-0.21}$	K 0
694	44.21	42.89	43.90	7.97	$1.89^{+0.02}_{-0.01}$	K 0
695	43.61	42.85	43.86	7.22	$1.72^{+0.15}_{-0.12}$	K 0
697	43.91	43.71	44.63	7.97	$1.75^{+0.11}_{-0.05}$	D 1
702	44.12	42.92	43.92	8.05	$1.74^{+0.05}_{-0.05}$	K 0
713	44.66	43.96	44.86	8.98	$1.57^{+0.17}_{-0.08}$	K 0
717	43.71	43.29	44.25	8.10	$1.82^{+0.10}_{-0.15}$	D 1
719	43.68	42.64	43.68	7.26	$2.13^{+0.01}_{-0.01}$	K 0
722	44.38	43.96	44.86	8.45	$2.05^{+0.23}_{-0.07}$	K 0
726	44.63	44.60	45.45	8.95	$1.78^{+0.12}_{-0.10}$	K 0
728	44.52	44.63	45.47	8.97	$2.18^{+0.11}_{-0.05}$	D 1
734	43.59	43.06	44.05	7.80	$2.00^{+0.06}_{-0.05}$	K 0
735	43.76	43.74	44.66	7.99	$2.14^{+0.04}_{-0.03}$	D 1
741	43.98	42.77	43.80	7.82	$1.82^{+0.29}_{-0.25}$	K 0
744	44.71	44.69	45.53	8.89	$1.86^{+0.50}_{-0.61}$	K 0
748	44.13	43.27	44.23	8.51	$1.86^{+0.07}_{-0.08}$	K 0
750	43.11	43.22	44.19	6.99	$1.96^{+0.19}_{-0.16}$	K 0
753	44.05	43.12	44.10	7.93	$2.00^{+0.03}_{-0.02}$	K 0
754	43.76	43.34	44.29	7.71	$1.65^{+0.10}_{-0.10}$	K 0
760	44.16	43.81	44.72	7.35	$1.99^{+0.18}_{-0.09}$	K 0
765	44.53	44.10	44.98	9.06	$1.65^{+0.37}_{-0.21}$	K 0
769	44.81	44.06	44.94	8.60	$1.74^{+0.28}_{-0.13}$	K 0
774	43.71	43.17	44.15	7.55	$1.78^{+0.07}_{-0.12}$	D 1
776	44.53	43.95	44.85	8.65	$1.74^{+0.31}_{-0.64}$	K 0
779	45.23	45.16	45.97	9.02	$1.61^{+0.16}_{-0.17}$	K 0
793	44.74	43.64	44.57	8.63	$1.73^{+0.11}_{-0.08}$	K 0
795	43.24	42.60	43.65	7.39	$1.74^{+0.09}_{-0.20}$	K 0
797	44.73	44.77	45.61	8.81	$1.92^{+0.09}_{-0.08}$	D 1
801	43.77	43.57	44.50	7.64	$1.60^{+0.09}_{-0.10}$	K 0
846	44.50	44.23	45.10	8.35	$1.71^{+0.12}_{-0.05}$	K 0
862	44.12	43.16	44.14	7.94	$1.63^{+0.12}_{-0.15}$	K 0
882	45.38	44.89	45.72	8.34	$1.98^{+0.12}_{-0.12}$	K 0
883	43.87	42.75	43.78	7.10	$1.74^{+0.11}_{-0.14}$	K 0
905	44.15	42.88	43.89	7.92	$2.09^{+0.06}_{-0.05}$	K 0
912	44.82	43.49	44.43	8.94	$1.73^{+0.09}_{-0.09}$	K 0
923	43.97	43.19	44.17	8.65	$2.12^{+0.28}_{-0.19}$	K 0
924	43.54	43.56	44.49	7.51	$1.51^{+0.09}_{-0.14}$	K 0
925	43.70	43.48	44.42	7.20	$2.29^{+0.14}_{-0.14}$	K 0
948	44.07	43.31	44.27	7.88	$1.52^{+0.12}_{-0.07}$	K 0
950	44.58	43.65	44.58	8.81	$1.70^{+0.11}_{-0.05}$	K 0
967	45.73	46.01	46.79	9.57	$2.22^{+0.03}_{-0.02}$	K 0
984	44.84	43.86	44.77	8.29	$2.07^{+0.02}_{-0.01}$	K 0
994	44.88	44.43	45.29	9.18	$1.74^{+0.06}_{-0.03}$	D 1
995	43.25	42.89	43.90	7.22	$1.94^{+0.05}_{-0.05}$	K 0
1013	44.72	43.81	44.72	8.40	$1.76^{+0.12}_{-0.11}$	K 0
1032	44.24	43.78	44.69	8.18	$2.05^{+0.11}_{-0.11}$	K 0
1036	44.06	43.94	44.84	9.02	$1.71^{+0.26}_{-0.22}$	K 0
1040	44.43	43.61	44.53	8.27	$1.86^{+0.21}_{-0.95}$	K 0
1041	44.23	43.99	44.88	7.99	$2.03^{+0.05}_{-0.05}$	K 0
1042	42.74	43.03	44.02	6.68	$2.44^{+0.07}_{-0.05}$	K 0
1043	43.75	42.81	43.83	7.35	$1.90^{+0.06}_{-0.09}$	K 0
1045	44.15	43.41	44.36	8.22	$1.91^{+0.10}_{-0.08}$	K 0
1046	42.68	42.12	43.24	6.42	$1.91^{+0.14}_{-0.10}$	D 1
1063	43.41	42.21	43.31	6.60	$1.70^{+0.08}_{-0.10}$	K 0
1084	43.79	43.13	44.11	7.21	$2.08^{+0.39}_{-0.47}$	K 0
1088	45.16	45.45	46.25	9.63	$2.04^{+0.16}_{-0.21}$	K 0
1089	44.01	45.43	46.23	8.42	$2.00^{+0.25}_{-0.16}$	K 0
1090	44.42	44.19	45.07	8.15	$1.67^{+0.09}_{-0.04}$	D 1

Table 1. –continu

ID	$\log L_{\rm x(14-195kev)}$ erg s^{-1}	$\log L_{5100}$ erg s^{-1}	$\log L_{\rm Bol}$ erg s^{-1}	$\log M_{\rm BH}$ M$_\odot$	Γ	Notes
(1)	(2)	(3)	(4)	(5)	(6)	(7)
1099	43.51	43.68	44.60	7.61	$2.22^{+0.45}_{-0.33}$	K 0
1102	44.79	45.08	45.90	8.96	$1.79^{+0.04}_{-0.04}$	K 0
1104	44.77	43.92	44.82	9.03	$1.84^{+0.16}_{-0.14}$	K 0
1106	43.90	43.52	44.46	8.48	$1.69^{+0.23}_{-0.19}$	K 0
1110	44.01	44.78	45.61	7.70	$1.82^{+0.11}_{-0.03}$	K 0
1117	43.51	42.51	43.57	7.23	$1.52^{+0.16}_{-0.08}$	K 0
1118	44.39	43.76	44.67	8.12	$1.79^{+0.13}_{-0.06}$	K 0
1120	45.24	45.27	46.08	9.45	$1.87^{+0.03}_{-0.03}$	K 0
1122	44.55	44.20	45.08	7.90	$1.74^{+1.34}_{-0.29}$	K 0
1132	45.05	45.55	46.35	8.99	$1.79^{+0.15}_{-0.11}$	K 0
1146	44.07	44.26	45.13	8.60	$1.95^{+0.40}_{-0.17}$	K 0
1151	44.56	43.54	44.47	8.11	$1.74^{+0.17}_{-0.18}$	K 0
1153	44.86	43.66	44.59	8.19	$1.67^{+0.08}_{-0.20}$	K 0
1162	43.37	43.62	44.55	7.72	$1.92^{+0.08}_{-0.08}$	K 0
1168	44.08	42.48	43.54	7.62	$1.49^{+0.51}_{-0.28}$	K 0
1172	45.01	44.49	45.34	8.52	$1.59^{+0.35}_{-0.05}$	K 0
1176	44.05	43.63	44.56	7.16	$2.18^{+0.15}_{-0.13}$	K 0
1178	43.81	42.97	43.97	7.05	$1.87^{+0.06}_{-0.06}$	K 0
1182	43.58	43.51	44.45	7.60	$2.09^{+0.14}_{-0.09}$	D 1
1183	44.77	43.70	44.62	8.66	$1.81^{+0.01}_{-0.01}$	K 0
1185	43.76	43.34	44.29	8.19	$1.57^{+0.13}_{-0.12}$	K 0
1187	44.17	43.59	44.52	8.64	$1.56^{+0.36}_{-0.24}$	K 0
1189	43.99	44.31	45.17	8.70	$1.88^{+0.03}_{-0.03}$	K 0
1195	44.81	44.37	45.24	8.52	$2.10^{+0.06}_{-0.03}$	K 0
1206	45.19	44.72	45.56	8.78	$1.78^{+0.35}_{-0.20}$	K 0